Reorganization of Binary Polymer Brushes: Reversible Switching of Surface Microstructures and Nanomechanical Properties

M. Lemieux,[†] D. Usov,[‡] S. Minko,*,[‡,§] M. Stamm,[‡] H. Shulha,[†] and V. V. Tsukruk*,[†]

Materials Science & Engineering Department, Iowa State University, Ames, Iowa 50011;
Institut für Polymerforschung Dresden, Hohe Strasse 6, 01069 Dresden, Germany; and
Department of Chemistry, Clarkson University, Potsdam, New York 13699-5810

ABSTRACT: For a binary polymer brush layer, we investigated the morphological state, the structure reordering, and the nanomechanical properties as a function of treatment with selective solvents. Two incompatible polymers, poly(methyl acrylate) (PMA) and poly(styrene-*co*-2,3,4,5,6-pentafluorostyrene) (PSF), were randomly grafted one after another onto a silicon wafer via the "grafting from" method producing thick (20−150 nm) dense mixed brush layers. The resulting layers possessed a nanostructured surface exhibiting either complete vertical or a combination of vertical and lateral microphase segregation of the two components. The lateral and vertical reorganization of the mixed brush layer was observed to be quick (on the order of a few minutes) and reversible for at least 100 "switches" between good and bad solvent states for each component. Atomic force microscopy (AFM) images revealed different surface structure states upon exposure to different solvents. Since PSF and PMA are mechanically dissimilar (glassy and rubbery, respectively) at room temperature, phase imaging was used to roughly verify the resulting structure. However, to determine vertical segregation in addition to truly authenticating the lateral ordering, surface nanomechanical mapping was conducted, which also allowed, for the first time, to directly determine the elastic modulus and adhesion. Results show the bimodal response of the mechanically heterogeneous surface, with elastic modulus and adhesion distributions very different for the "glassy state" and the "rubbery state". Furthermore, depth profiling of the elastic modulus conducted for binary brushes confirmed the vertical segregation in the mixed brush. Results demonstrated the dramatic mechanical contrast of the surface as a function of solvent conditions and decisively revealed the modes of phase segregation in a binary polymer brush.

Introduction

Sophisticated, next generation micromechanical systems, capable of working in fluctuating "wet" environments, require adaptive surfaces constructed with "smart" properties that can not only sense or respond to environmental stimuli but also be robust and possess tailored, on-demand physical properties.[1] Polymer brush films, with their ability to change surface structure under external stimuli, are prospective materials for these applications. Irreversible (chemical) or reversible (physical) grafting of polymer chains to a flat solid interface generally results in one of three possible conformations depending upon grafting density of the chains.[2,3] At low surface concentrations, the chains lie on the surface and form the "pancake" structure. As concentration increases, the "mushroom" conformation appears until a threshold is reached at which point the grafting density becomes high with respect to the free radius of gyration (R_g) of the polymer chain, and the "brush" structure is prevalent.[4] The most intriguing of these structures is the brush structure in which one end is strongly tethered to the solid interface, and the rest of the chain attempts to alleviate overlapping by stretching away from the surface so that the equilibrium conformation is a highly stretched conformation.[5,6] This conformation, where the chain stretching is considerably larger than the R_g (especially in the presence of a good solvent), is quite different from typical flexible polymer chain behavior in the isotropic bulk state in which the random-walk (Gaussian coil) configuration is found.

Numerous theoretical and experimental papers are dedicated to thin polymer films with the brush architecture.[7−9] As a result of the high grafting density and uniformity in composition and chain height throughout the brush, the layer responds communally to very subtle changes in the surrounding environment such as pH,[10] temperature,[11] and solvent quality.[12−14] Thus, the brush structure is responsible for physical properties important in applications of colloid stabilization,[15] drug delivery and biomimetic materials,[16,17] chemical gates,[18] and tuning lubrication, friction, adhesion, and wettability for tailored surfaces.[19−21] In the case of two-component or binary polymer brush layers, the variety of surface morphologies possible greatly increases depending upon the chemical composition. Surface composition and hence properties such as surface energy, adhesion, friction, and wettability have the possibility of being "tuned" to the necessary state.

On the basis of self-consistent-field (SCF) theory, it was proposed that the grafting of two incompatible polymers at high densities produced either a "layer profile" or a "ripple profile".[22] The layered profile describes a vertically segregated system where only one of the components is found at the top and the other at the polymer/inorganic interface. The case when both

[†] Iowa State University.
[‡] Institut für Polymerforschung Dresden.
[§] Clarkson University.
* To whom correspondence should be addressed. E-mail: minko@ipfdd.de; vladimir@iastate.edu.

components are equally found at the top layer of the brush with a nanodomain structure describes the ripple profile. While it is known that sufficiently random, irreversible grafting of incompatible polymers prevents lateral macrophase separation, the ripple profile describes a system in which the two components are laterally segregated, with the dimensions of the lateral structures on the order of the free radius of the chains.[22] The ripple profile is found commonly in block copolymers where well-defined, two-dimensional nanostructure morphology is prevalent. Additionally, Soga et al. have also shown that lateral microphase separation dominates in a mixed brush of two incompatible species for a *nonselective* environment.[23] The vertical layered profile has been predicted in some cases as described by Brown et al.[24] Recently, a phase diagram has been proposed for a binary polymer brush.[25] It was found that in systems with high incompatibilities a never before seen "dimple phase" is thermodynamically stable when the system is exposed to selective solvents. When the solvent quality is decreased for species A, this species collapses and forms round A clusters that supposedly arrange in a hexagonal lattice.[25]

There are two conventional methods for the fabrication of polymer brush layers: the *grafting to* approach and the *grafting from* approach. The grafting to approach involves preformed, end-functionalized polymers reacting with a suitable surface under appropriate conditions to form a tethered polymer brush.[2,3,26−28] To facilitate the strong chemical attachment, the substrate is modified with a reactive precursor acting as coupling agents such as functionalized self-assembled monolayers (SAMs).[29−32] While being less complex than the grafting from approach, the grafting to approach is hampered by steric constraints and kinetic factors. Slowing diffusion of additional long chains through the existing polymer film prevents reaching the high grafting density. Moreover, space constraints around these potential reactive sites further limit the grafting density.[27,32,33] This barrier becomes even greater as the layer thickness increases, and the process becomes self-limiting. Therefore, the amount of grafted polymer is usually in the range of 2−10 mg/m^2, although this still should be on the concentration edge to create the brush structure.[2,6,34]

The brush layers presented in this study have been synthesized via the grafting from approach. In fact, to increase grafting density, radical polymerization *from* the substrate has been used in the past decade as an alternative method from the grafting to approach for creating highly dense brushes of high molecular weight.[35−37] The grafting from approach starts with the application of an immobilized radical initiator attached to the substrate via SAMs, followed by surface-initiated polymerization to form a tethered layer. Using this approach, some authors have reported high grafting densities in the range of 15−100 mg/m^2 and brush layer thickness on the order of 100 nm.[38−40]

In our previous work, we have shown that thick (50−90 nm) homopolymer brushes of poly(methyl acrylate) (PMA) and poly(styrene-*co*-2,3,4,5,6-pentafluorostyrene) (PSF), synthesized via the grafting from approach produced dense, homogeneous brush layers.[41] The physical properties of these brushes were characterized and found to be very different for each layer, which is expected since PSF is glassy at room temperature (glass transition temperature, T_g, is 109 °C), while T_g for PMA is around 5 °C.[41] Young's modulus of the homobrush

layers was approximately 1 GPa and 50 MPa for PSF and PMA, respectively. Furthermore, the adhesive forces were more than 5 times higher for PMA, containing highly polar segments, than with the fluorine-enriched PSF.[41] Here, we combine these two very different polymers into a binary brush layer to create a modified surface with the possibility of possessing varying morphological states and hence tunable physical properties. We directly reveal the reversible switching morphology of a binary brush surface sensitive to changing solvent conditions with atomic force microscopy (AFM). Furthermore, we aim to quantify the mechanical properties at the nanoscale associated with each morphological state. All experiments are done in the dry state; however, there is much evidence that the dry morphology is closely associated with the same morphology under solvent.[42] After exposure to a solvent, the film was dried in approximately 1 s under dry N$_2$. Thus, the time for solvent evaporation is tremendously smaller than the time needed for switching (minutes), and it is reasonable to suggest that the morphology observed in dry brushes reflects that under solvent.[42] In our case, this suggestion has been experimentally verified as AFM results reveal that morphology under toluene and acetone correspond well to the respective dry states in terms of the level of lateral and vertical segregation in each as will be discussed in a separate publication.

Only a few studies have been conducted to verify the theoretical models discussed above, and there has been no study to date addressing the physical properties associated with morphological changes of such a layer. The earlier work, using several methods including AFM, contact angle measurements, and XPS, experimentally verified the switching of binary polymer brushes exposed to different solvents and provided direct data to prove that indeed the surface chemical composition could be switched and that the surface composition can be precisely tuned.[26,34,42] The evidence of the dimple phase was also produced using AFM.[43] To our knowledge, this paper presented here is the first experimental work that verifies the complete reversible switching of elastic and adhesive properties at the nanoscale in a polymer film and provides detailed results justifying a model of structural reorganization that includes both lateral and vertical segregation of dissimilar polymers.

Experimental Section

Materials. *Monomers.* Styrene (S, Aldrich), 2,3,4,5,6-pentafluorostyrene (FS, Fluka), and methyl acrylate (MA, Aldrich) were purified with an aluminum oxide type 507C, neutral, 100−125 mesh (Fluka) chromatographic column. Solvents of analytical grade toluene, tetrahydrofuran (THF), and hexane were distilled after drying with sodium. Dichloromethane was dried over molecular sieves overnight, and methanol and ethanol were used as received.

Initiators. 4,4′-Azobis(4-cyanopentanoic acid) (ABCPA, Aldrich) and 4,4′-azobis(isobutyronitrile) (AIBN, Fluka) were purified by recrystallization from methanol. All reagents were used immediately after purification. Water was cleaned with a Milli-Q ultrapure purification system, Ω >18.0 Mohm cm. Silicon wafers (Wacker-Chemitronics GmbH, Burghausen, Germany) were cleaned with dichloromethane and then in an ultrasonic bath mixture of NH$_3$ (25%), H$_2$O$_2$ (30%), and water in the ratio 1:1:10 at 60 °C and were rinsed several times with water. 3-Glycidoxypropyltrimethoxysilane (GPS, Aldrich), ethylenediamine (ACROS Organics), and phosphorus pentachloride (Merck) were used as received. Triethylamine (Riedel-deHaën) was dried on calcium hydride.
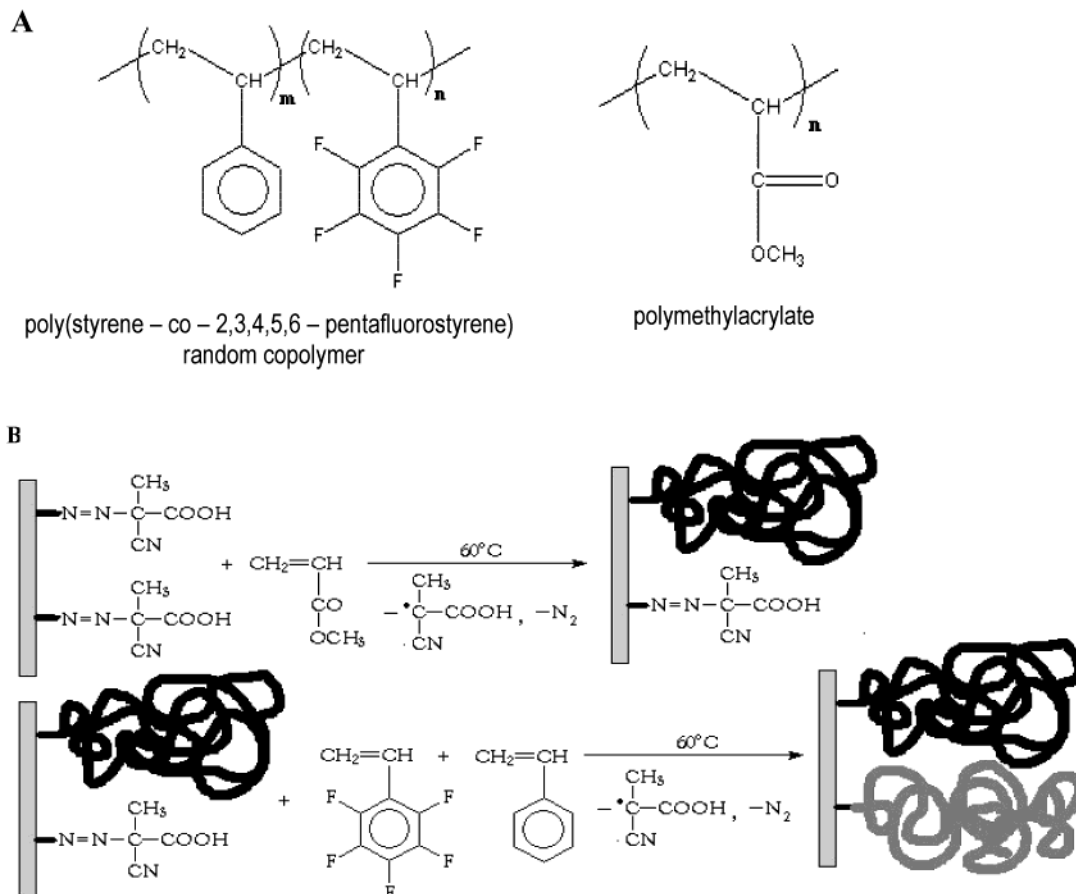
Figure 1. (A) Chemical structure of the two polymers in the binary brush. (B) Scheme of the two-step synthesis of PMA (black chains) and PSF (gray chains) from the silicon substrate using the azo-initiator.

Introduction of Azo-Initiator. Silicon wafers were treated under an Ar atmosphere by 1% GPS in dry toluene for 16 h and afterward washed two times with dry toluene under Ar and three times with ethanol in an ultrasonic bath. In the second step, the Si wafers were treated with 2% ethylenediamine in ethanol for 1 h and washed three times with ethanol. Separately, a chloroanhydride derivative of ABCPA (Cl-ABCPA) was prepared. A suspension of 5 g of ABCPA in 50 mL of $CHCl_3$ and a slurry of 40 g of PCl_5 in 100 mL of $CHCl_3$ were mixed at 0 °C under an Ar atmosphere. The mixture was stirred overnight under an Ar atmosphere while it warmed to room temperature. CH_2Cl_2 was evaporated out under reduced pressure to precipitate the major part of the dissolved PCl_5. The yellow solid of PCl_5 was filtered off. Cl-ABCPA was precipitated at 0 °C as a white powder in 300 mL of dry cold hexane, filtered and washed with dry cold hexane, and dried in a vacuum, giving 84% yield. In the next step, Cl-ABCPA was introduced on the surface of the Si wafers from 1% solution in dichloromethane with a catalytic amount of triethylamine at room temperature under an Ar atmosphere for 2 h. The resulting samples of Si wafers with chemically attached initiating groups were rinsed with dichloromethane under Ar and then with ethanol in an ultrasonic bath. Every step of the modification of the Si wafers was controlled by ellipsometry measurement of the layer thickness.

Graft Polymerization. We grafted PMA at the first polymerization step and then PSF at the second step using the residual amount of the azo-initiator on the Si substrates (Figure 1). Oxygen was removed from the monomer solution (MA in toluene, 5 mol/L, or a mixture of S and FS in ratio 4:1 wt in THF, 5 mol/L, and AIBN, 4.4×10^{-4} mol/L) using five freeze−pump−thaw cycles. The Si wafers with the chemically attached azo-initiator were placed into a reactor with the monomer solution under an Ar atmosphere. The reactor was immersed in a water bath (60 ± 0.1 °C) for 12 h. This time of polymerization was determined on the basis of the kinetics of

decomposition of the azo-initiator. Relatively slow decomposition of the azo-initiator (half-life of 21 h at 60 °C) allows for the two-step grafting from the surface as has been demonstrated in our previous publications.[34,36,37] The Si wafers were rinsed several times with toluene. The nongrafted polymer was removed by cold Soxhlet extraction in THF for 1 h. The same procedure was used to graft the second polymer. The nongrafted amount of the second polymer was removed by a hot Soxhlet extraction in THF for 12 h. Since complete extraction of the ungrafted chains is a critical issue in this system, we have studied extensively the ungrafted polymer extraction and found that layer thickness does not change significantly after 4 h of extraction time, which indicates complete removal of ungrafted polymers under selected experimental conditions. The grafted amount of the polymers was controlled after each polymerization step with ellipsometry. These studies were based on ellipsometry measurements of the grafted layer up to 40 h of extraction time, as was discussed in detail earlier.[36,37] For additional testing, throughout the course of this study spanning several months, the brushes were washed in different solvents followed by ultrasonication several times with essentially no change in thickness and complete reproducibility results after these treatments.

Switching of the Binary Polymer Brushes with Solvents. A sample was immersed in the selective solvent (toluene or acetone) for 5 min and then rapidly dried under a nitrogen flux. Water contact angle measurements were conducted with the sessile drop method using Nanopure water on a custom-made system. Droplets of roughly 5 μL of Nanopure water were placed on the surface, and the contact angle was measured in less than a minute using a microscope equipped with a digital camera. The shape and angle of the drop were analyzed with software. Contact angle measurements showed that the time of switching of the binary brush was usually in the range of several minutes. Confirmation of

Table 1. Characteristics and Parameters of Grafting for the Polymers in the Binary Brush

brush	polymer	M_w (g/mol)	M_n (g/mol)	R_g (nm)	polydispersity index (M_w/M_n)	ellipsometry thickness[a] (nm)	grafted amount (mg/m²)	grafting density (chain/nm²)	grafting distance (nm)
PMA + PSF	PMA	505 000	121 000	10.0	4.2	24.0	25.2	0.13	3.1
	PSF	372 000	219 000	13.4	1.58	36.0	43.2	0.12	3.3
	PMA + PSF	NA	NA	NA	NA	60.0	68.4	0.15	2.9

[a] Data for dry state of polymer brushes for each step of grafting after treatment with THF.

changed chemical composition of the topmost layer was obtained with XPS as well.

Characterization of the Brush Layers. The amount of the chemisorbed initiator and the grafted amount of polymers was measured with ellipsometry. Film thickness was measured using a COMPEL automatic ellipsometer (InOm Tech, Inc.) at 70° angle of incidence with the values of refractive indices determined for the thick films according to the known procedure.[31] For data interpretation, a multilayer model of the grafted films was used as it was described elsewhere.[34] For calculations, we used the following values of the refractive indices: for the epoxy-terminated SAM $n = 1.429$ and for the SAM and attached azo-initiator an effective value of $n = 1.55$. For the relatively thick polymer layers (thicker than 30 nm) the refractive indices were obtained directly from the ellipsometry experiments.

The molecular weight of the grafted polymers was evaluated with GPC plots completed on a Breeze 1500 instrument (Waters) using polystyrenes as calibration standards assuming that the polymers in the bulk have the same molecular weight as the polymers grafted to the substrate. There are contradictory reports in the literature concerning this assumption. The kinetics scheme suggests almost the same molecular weight for grafted chains and chains in the bulk,[36] but in some experiments an increased molecular weight and larger polydispersity index for the grafted polymer as compared to the bulk polymer was documented due to the Trommsdorff effect.[35,38] The composition of the random copolymer poly-(styrene-*co*-2,3,4,5,6-pentafluorostyrene) (P(S-*co*-FS)) was calculated from ¹H NMR spectra, and for all samples it was S:FS = 75(±2):25(±2).

Topographical and phase images of the surface morphology were observed under ambient conditions in the tapping mode using a Dimension 3000 and Multimode microscopes (Digital Instruments, Inc.). For imaging, silicon tips with radius of 10–30 nm were used with spring constants ranging from 1 to 30 N/m. Scan rates typically ranged from 0.7 to 1.5 Hz, and exerted forces did not exceed several nanonewtons in "light" tapping mode. For the high-resolution scans, the tip radius was measured to be 10 ± 1 nm, with scan rates of 0.5–0.9 Hz for scans of 200–900 nm. Tapping mode was used according to the well-established procedure adapted in our lab.[44] Force volume mode, which utilizes the collection of the AFM force–distance curves (FDC) over selected surface areas, was used for micromechanical analysis (MMA) of the binary polymer brush layers. A single FDC records the forces acting on the tip as it approaches to and retracts from a point on the sample surface.[45] Force volume mode allows for the micromapping of the mechanical properties of polymer surfaces with nanometer scale resolution, while obtaining topographical information simultaneously.[46,47] Typically, we used 64 × 64 or 32 × 32 pixels within 1 × 1 or 2 × 2 μm surface areas to do micromapping with a lateral resolution of 15 nm. Data collected were processed using an MMA software package developed in our lab which provides means for calculation of localized elastic modulus, depth profile of elastic modulus, reduced adhesive forces, and surface histograms of elastic moduli and adhesive forces from experimental images as described elsewhere.[48] Spring constants of cantilevers were determined from the resonant frequencies and the tip-on-tip method according to the procedures described earlier.[49,50] Tip radii were evaluated with scanning of reference gold nanoparticle specimens in combination with a deconvolution procedure.[51,52] The tips used for MMA were either silicon or silicon

nitride with radius of 15–60 nm and spring constant ranging from 0.5 to 10 N/m.

Results and Discussion

Chemical Composition and Grafting Density. The thickness and grafting density of the polymer brush layers were controlled by terminating the reaction after 12 h. For these studies, we chose a grafting amount of approximately 25 mg/m² for PMA and 43 mg/m² for PSF (Table 1), which are typical for the grafting from approach.[34] The thickness of the polymer layers measured with ellipsometry after each grafting step was about 24 nm for PMA layer and 36 nm for PSF layer (Table 1). These values are much higher than typical grafting densities and thicknesses than can be achieved by the grafting to technique. The molecular weights (M_w and M_n) determined from GPC (Table 1) for the PMA and PSF obtained concurrently via bulk polymerization under identical conditions have values of 505 000 and 121 000 (g/mol) (PMA) and 372 000 and 219 000 (g/mol) (PSF). The polydispersity of both polymers is quite modest and close to the expected values (4.2 for PMA and 1.58 for PSF). The molecular weight of these polymers can serve as a guide for the evaluation of the anticipated molecular weight for grafted brushes under assumption of close correlation of the grafted polymers and the bulk polymers.[36]

The anticipated grafting density (D, chains/nm²) of the brush layers was evaluated from M_n and the layer thickness (d, nm) according to the formula $D = d\rho N_a/(M_n \times 10^{21})$, where ρ (g/cm³) is density of the polymer and $N_a = 6.022 \times 10^{23}$ (mol⁻¹) is Avogadro's number.[27] The end-to-end distance (h_Θ, nm) of an unperturbed polymer chain in bulk state was calculated from $h_\Theta = kM_n^{0.5}$, where k was taken to be 0.068 for PMA and 0.070 for PSF.[53] The radius of gyration, R_g, was calculated as $h_\Theta/\sqrt{6}$. The grafting density was estimated to be close to 0.1 chain/nm², which is high for these very long-chain macromolecules. Indeed, the anticipated average distance between grafting points, l, calculated as $l = 2(\pi D)^{-0.5}$ was close to 3 nm for both polymers, which is an indication of the extremely high grafting density (Table 1). Considering a diameter of the macromolecules of 20–30 nm, we can conclude that more than 100 chains are strongly overlapped within a volume occupied by a single grafted macromolecular chain. In addition, even in a dry state, significant stretching is expected for the PSF brushes where the layer thickness was twice larger than the macromolecular diameter and modest stretching (60%) is anticipated for rubber PMA macromolecules.

Switching in Different Solvents and Surface Morphology. Initially, switching of the surface was evident with water contact angle and optical measurements (Table 2, Figure 2). The contact angle varied from 95° to 100° in the glassy state and in the range of 117–122° in the rubbery state over 15 measurements for each of three cycles of switching. This correlates well with

Table 2. Physical Properties of Individual Components and the Binary Brush[a]

polymer	T_g (°C)	contact angle (deg)	overall elastic modulus (MPa)	overall adhesion (mJ/m²)
PMA homopolymer	5	84	6−50	NA
PSF homopolymer	109	99	800−1200	NA
PMA + PSF rubbery state	NA	117−122	30−60	110
PMA + PSF glassy state	NA	95−100	500−900	80

[a] Data for PSF and PMA homobrush layers are taken from ref 41.
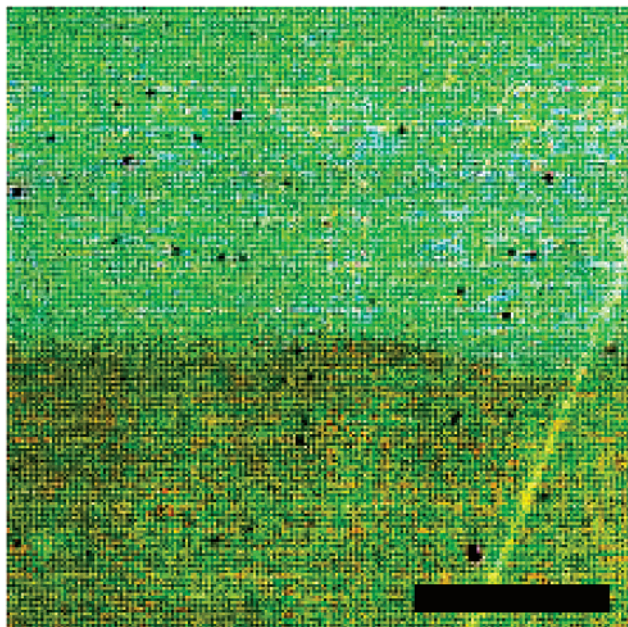
Figure 2. Optical micrograph demonstrating the optical effect of switching can be observed macroscopically. The upper part of the brush (blue) was treated with acetone, and the lower part (yellow−green) was exposed to toluene. Bar is 1 mm.

values found for PSF, but not PMA homobrushes, which were 99° and 84°, respectively.[41] The larger variations in the rubbery state can be attributed to the higher surface roughness as compared with the glassy state, and the 115°+ values are reasonable even on extremely hydrophilic surfaces due to the excessive surface roughness (30 nm rms for rubbery state).[54]

Two very different morphologies appeared when the brush layer was exposed to toluene and acetone (Figures 3 and 4). The images of different morphologies were done using the same AFM tip so direct comparisons could be made. It is known that acetone is a selective solvent for PMA, and toluene is the selective solvent for PSF.[4] Thus, two different states or morphologies are possible. Accordingly, the following nomenclature will be used through the rest of this paper: (1) the *glassy state*, which should result after toluene exposure with PSF expected to be on the top layer, and (2) the *rubbery state* should be formed after acetone exposure since PMA is expected to swell and be enriched at the top of the brush.[4,14]

Indeed, imaging of binary brushes after different solvent treatment reveals the enormous height difference between the two states (Figure 5). In addition, surface microroughness (measured within a 1×1 μm surface area) increased from 2.2 ± 0.5 nm in the glassy state to 28 ± 4 nm for the rubbery state. In the rubbery state, PMA seemingly swells to a high degree forming
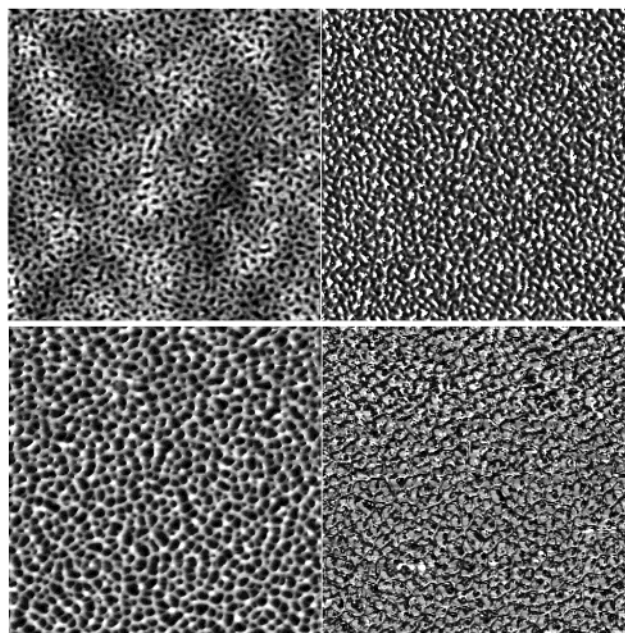

Figure 3. AFM images (left, topography; right, phase) of the glassy (top) and rubbery (bottom) state of the binary brush at 5×5 μm in the soft tapping regime. Top picture: Z scale for height is 10 nm, Z scale for phase is 20°. Bottom picture: Z scale for height is 150 nm, Z scale for phase is 40°.
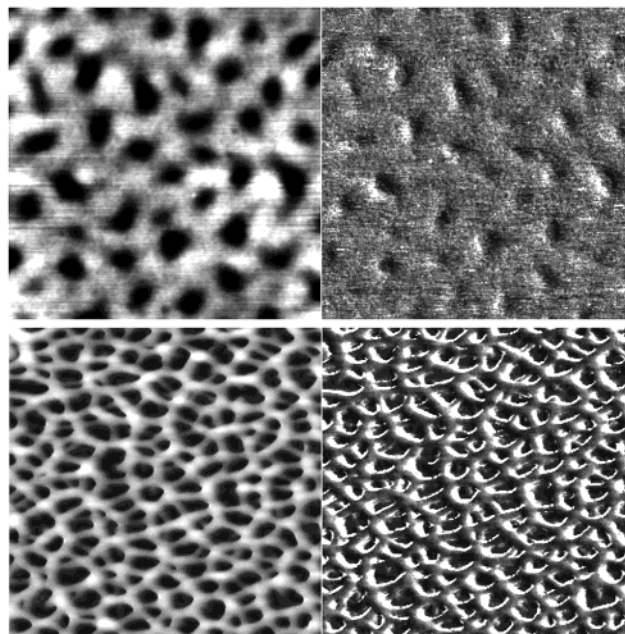

Figure 4. AFM images (left, topography; right, phase) of the glassy (top) and rubbery (bottom) state of the binary brush at 1×1 μm in the hard tapping regime. Top picture: Z scale for height is 10 nm, Z scale for phase is 20°. Bottom picture: Z scale for height is 150 nm, Z scale for phase is 40°.

a weblike cellular layer over the collapsed PSF, whereas in the glassy state, PSF forms a thin layer over the collapsed PMA. It appears that changes in vertical reordering dominate the pattern of binary brush in selective solvents. The pronounced vertical segregation (layering) is in agreement with previous experiments and theoretical calculations, although it is unclear from height images alone whether clusters (dimples) are forming underneath the swelled component, as would be expected.[43] The fact that the rubbery state swells approximately 10 times higher than the glassy state can
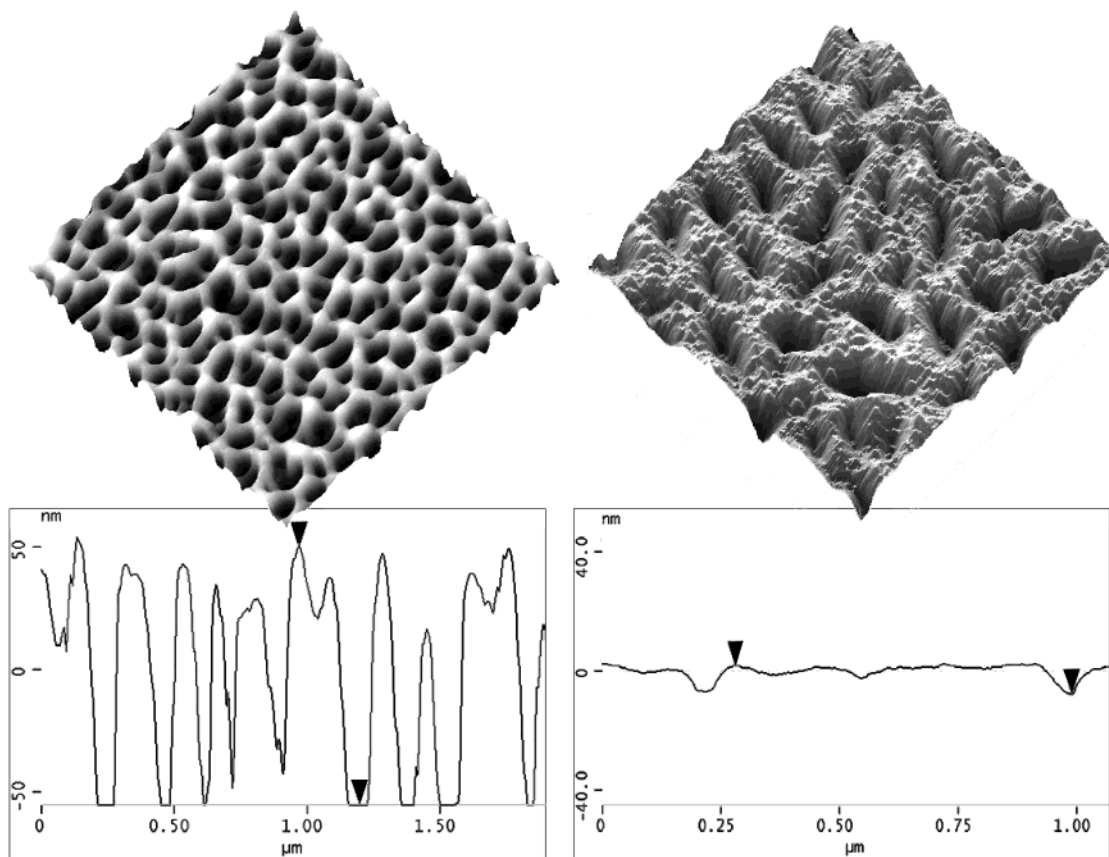
Figure 5. Three-dimensional surface plots and corresponding profile analysis of the rubbery (left, height increment is 50 nm) and glassy state (right, height increment is 40 nm) showing the immense difference of height and surface roughness between the two states. The profile for the glassy state shows that two types of depressions in the PSF layer are found: large (8−10 nm deep) and small (1−7 nm deep).

be attributed to two reasons. First, the Flory interaction parameter is more favorable for the PMA−acetone combination rather than PSF−toluene mixture. Second, the high glass transition temperature (T_g) makes PSF far less mobile than PMA chains under comparable time and temperature conditions.

Topographical images confirm that lateral phase segregation does not occur for dimensions significantly larger than the R_g, meaning the grafting sites for each component are sufficiently uncorrelated. The switching between the two morphologies presented in Figures 3 and 4 is reversible for at least 100 switches, and each state remained stable for long periods of time (several months) in ambient conditions.

For a nanostructured surface, phase imaging is instructive for identifying different domains because phase contrast (phase shift) is a result of differences in energy dissipation from each tip−sample interaction.[55] Thus, constituents in the surface with varying compliance, adhesion, and viscoelasticity will produce phase contrast. Phase imaging is also able to identify subsurface domains.[28,56] For practical scanning, the set point ratio (rsp), defined as the ratio of operating set point (amplitude) to the free oscillating amplitude of the cantilever, must be taken into account for correct interpretation of phase images as was proposed by Magonov et al. in the terms of two regimes.[56] The attractive regime, or light tapping, is characterized by an rsp of 0.9−1, while the repulsive regime, or hard tapping, has an rsp of 0.4−0.7. In light tapping, the tip−sample interaction is strongly influenced by adhesion, and the phase shift is greater on the surface with areas
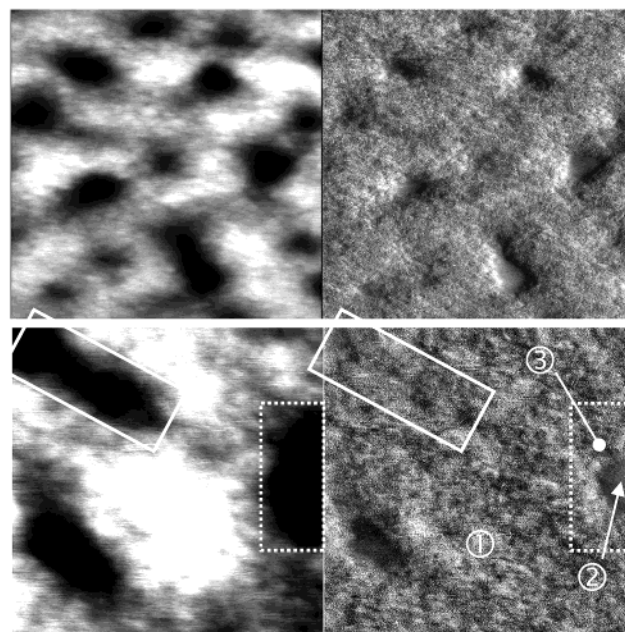

Figure 6. High-resolution tapping mode images of the glassy state morphology in the hard tapping regime. Top: 400 × 400 nm, height Z scale is 10 nm, phase Z scale is 20°. Bottom: 200 × 200 nm, height Z scale is 10 nm, phase Z scale is 20°. White solid rectangle indicates depression in the PSF layer as phase is unchanged from the surrounding area, while the white dashed rectangle indicates a complete hole in the PSF layer with the change in phase indicating the presence of the compliant PMA. The numbers in phase correspond to different force distance points in the mechanical properties discussion.
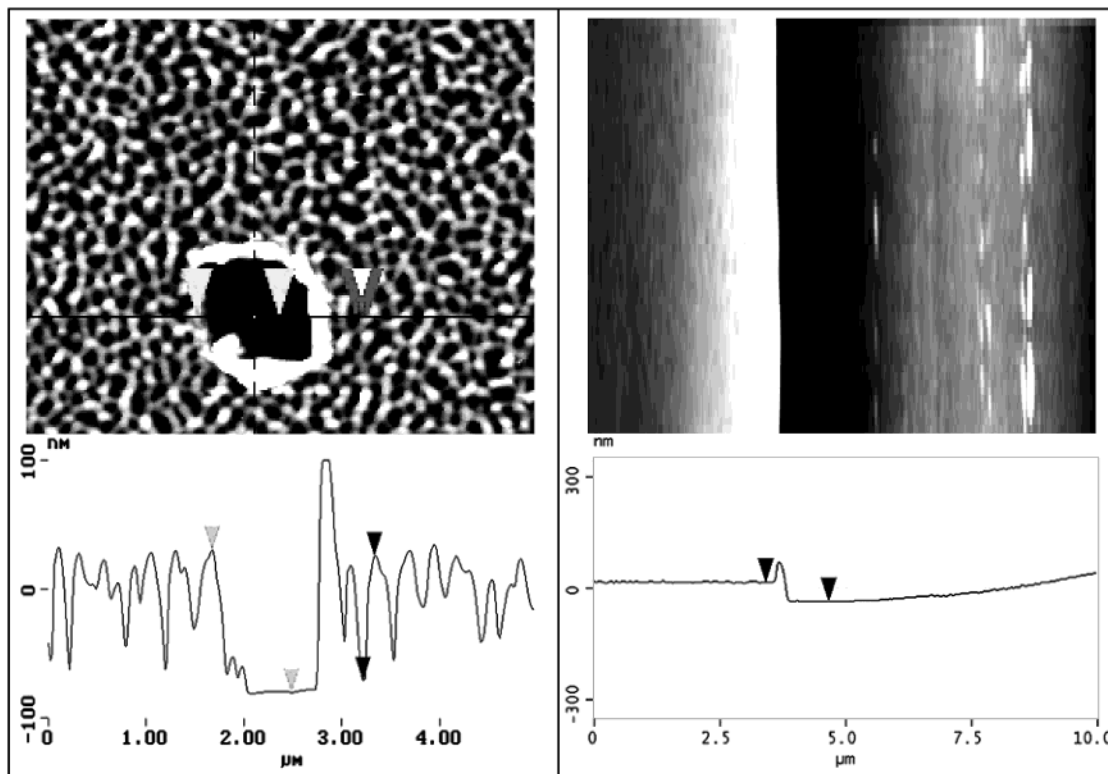
Figure 7. Results of AFM scratch test of the rubbery state (left) and the glassy state (right). For the rubbery state (top left), scanning was done in contact mode at harsh conditions (high forces), removing all polymer and exposing bare silicon. Sectional analysis (bottom left) from subsequent zoomed out tapping mode scan reveals greatest thickness of PMA (black arrows) to be around 100 nm, while the total thickness was 115 nm (gray arrows), meaning that PSF thickness in the collapsed state is around 15 nm. For the glassy state (right), PSF was more difficult to remove, and a sharp tool was used to create the scratch. After flatten and plane fit of the image (top right, image appears distorted due to aspect ratio scanning), the thickness of the layer (black arrows, lower right) was close to 50 nm. Combining this with the glassy cross-section analysis (Figure 5) where PMA was observed only in the deepest holes of 10 nm, collapsed PMA has apparent thickness of 30−40 nm in the glassy state.

of higher attractive forces whereas in the hard tapping regime the elastic response becomes predominant.[55]

The AFM images in Figure 3 were scanned using light tapping. For the glassy state, the brighter areas in phase correspond to the holes in the height image that can be associated with presence of predominantly PMA material within holes. Tentatively, it can be thought that the glassy PSF chains vertically segregate to the top around the compliant PMA, which forms clusters, and the tops of these clusters are observed as the phase contrast. However, the phase shift is very minor (only several degrees) and can be also affected by a topographical contribution. Thus, only from AFM images we *cannot conclude unambiguously* whether the holes seen in the glassy state are depressions in the PSF layer or actually the tops of soft PMA clusters. Micromechanical analysis (MMA) needs to be conducted before final conclusion (see below). Interpretation of the rubbery state is more straightforward as the phase images in Figures 3 and 4 show a very homogeneous top layer (except some topographical contribution from the edges). The conclusion can be made that the rubbery PMA dominates the top layer of the brush after exposure to acetone.

In the hard tapping mode, the stiffer domains appear brighter in phase while the more compliant regions are dark.[28,55] Figure 6 shows progressively high-resolution images for the glassy state. The holes in the 400 nm scan correspond to dark shifts in the phase image, although close inspection reveals some depressions in topography have no phase contrast. The 200 nm image

clarifies this ambiguity. The hole in topography surrounded by the solid white box in Figure 6 appears the same as the hills in phase. However, the hole type highlighted by the dashed box shows two regions in phase: at the edges of the holes there is no phase contrast, and only at the deepest region a darker shift in the phase image seemingly indicates the compliant PMA.

Switchable Mechanical Properties of Binary Polymer Brush Layers. Analysis of the AFM imaging results in combination with AFM scratch tests, which is a method for extracting the thickness of each component in the mixed brush (Figure 7), seems to confirm the mode of reordering between the two states and identification of phases in each state. Micromechanical analysis (MMA) of the binary brush layers after exposure to different solvents is the next step and provides additional information in terms of surface elasticity that can be useful for the identification of different phases. It can *directly determine* whether there is switching of the elastic properties associated with the changed morphology discussed above. Micromapping of the binary polymer brushes has proven to be a difficult task for several reasons. First, because of the nanodomain phase separation, high lateral resolution is necessary, which means a very small tip radius must be used. Because of the calibration of the cantilever sensitivity that consists of repeated normal contact with silicon, as well as the repeated penetration into polymer layers, the tip can become blunt and contaminated rather quickly. Accurate force volume measurements greatly depend on accurate calibration of the sensitivity, and
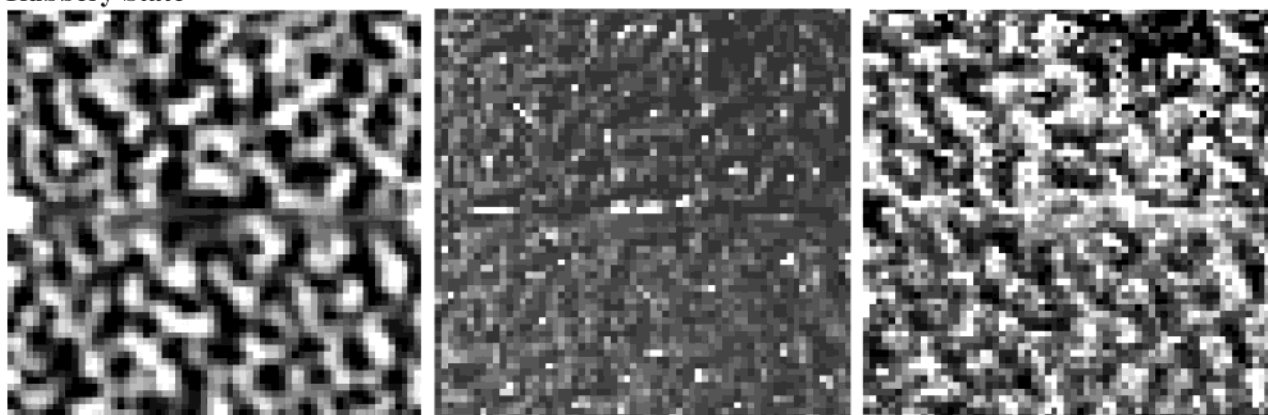
Glassy State
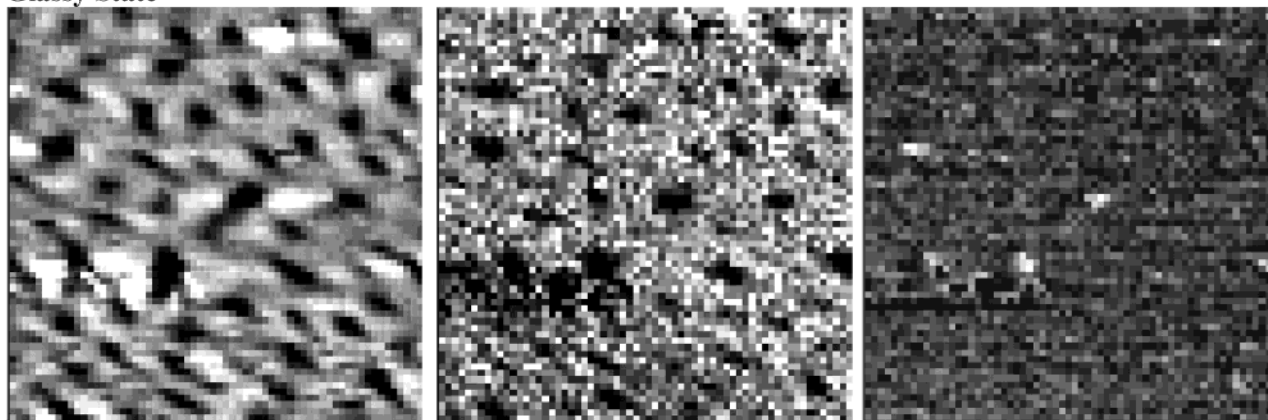
Rubbery State

Figure 8. Force volume images at 64 × 64 resolution at 1 × 1 μm for the glassy state (top row) and 2 × 2 μm mapping for the rubbery state (bottom row). Topography (left column), elastic modulus (middle column), and adhesive force (right column) distributions are presented. Bright areas correspond to higher topography, elastic modulus, and adhesion.
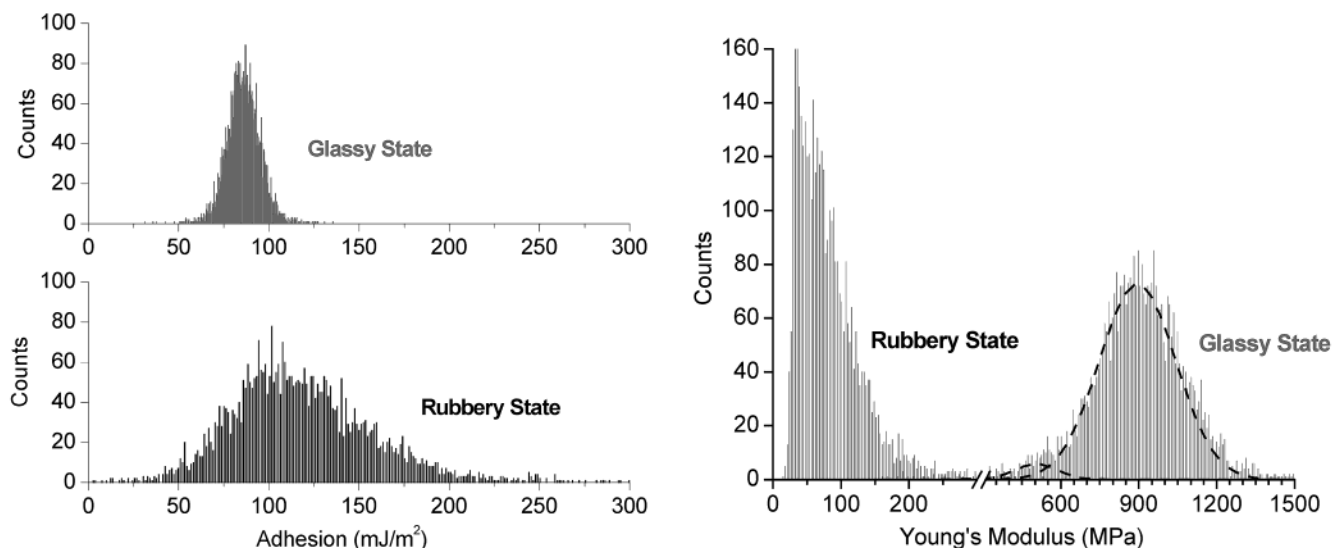

Figure 9. Surface histogram distributions from MMA mapping demonstrating the mechanical (adhesion, left; elastic modulus, right) difference of by the binary brush layer in two separate states. Histograms are taken from 64 × 64 force volume scans for a total of 4096 data counts. The elastic modulus is the average value for each data point over the entire indentation range. The histogram representing the modulus in the glassy state shows a bimodal distribution fitted with two Lorentzian functions.

confirming the constant sensitivity of the cantilever without greatly altering the tip radius is a challenge. Second, PSF and PMA are expected to have contrasting mechanical properties. It has been determined that only a small range of cantilevers, in terms of spring constant and, hence, local pressure, are applicable to probe the surface nanomechanical properties of a given polymer.[57] Since we have a glassy and a rubbery polymer within the same probing area, it is difficult to find a perfectly matched spring constant to probe both. Accordingly, force volume probing was repeated several times using stiffer and softer cantilevers to achieve higher sensitivity for either glassy or rubbery surface areas.
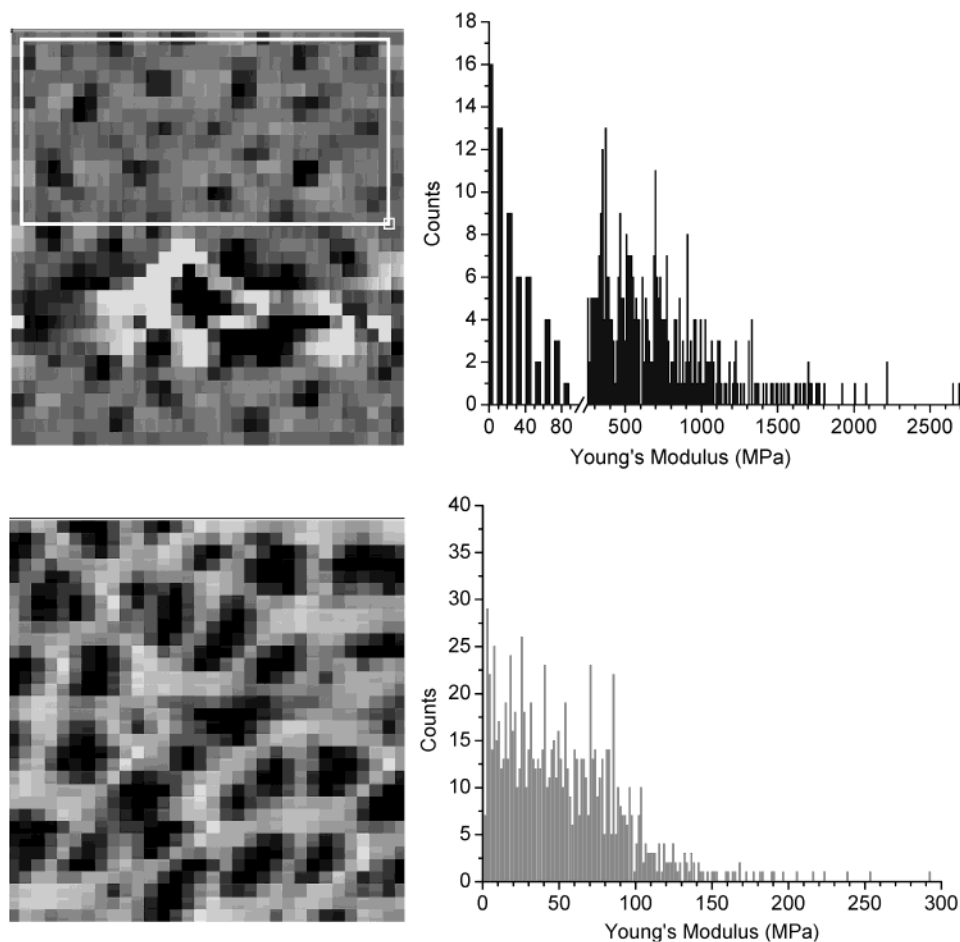
Figure 10. Force volume topography distribution and corresponding elastic modulus histograms from the glassy (top row) and rubbery state (bottom row) using a soft tip. The histogram in the glassy state was derived from the region with the white frame to avoid incorrect data from the damaged surface region. The bimodal distribution is enhanced in the glassy state. Histograms are taken from 32 × 32 force volume scans at 1 × 1 μm.

Force−volume probing produces a micromapping of the surface elastic and adhesive properties with lateral resolution of 10−30 nm (Figure 8, Table 2). MMA of the glassy state showed a mechanically heterogeneous surface in contrast to a homogeneous surface in the rubber state. For the glassy state, the holes correspond to areas of low elastic modulus and increased adhesion, evidence of a more compliant and sticky rubbery PMA material. The surface histogram of elastic modulus and adhesive forces presented shows a bimodal distribution of the elastic modulus that is expected for a surface with microphase-separated regions (Figure 9). The value of the main maximum of 900 MPa is close to the measurement on PSF homopolymer brush (1.1 GPa) and is typical for brush layers of glassy polymers.[41] A minor contribution of about 480 MPa originates from holes and indicates a softer but still relatively stiff surface. On the other hand, for the rubbery state, the elastic modulus was within a narrow range of values, 50−100 MPa, typical for a rubbery polymer and indicating a more complete and homogeneous, soft top layer. Elastic modulus histograms were also obtained using a softer tip with higher sensitivity (Figure 10). The glassy state shows an even more amplified bimodal distribution than that with the stiff tip. Individual measurements are distributed in the range 10−50 MPa (characteristic of PMA domains) and 400−1000 MPa (characteristic of PSF domains).

Examination of individual force−distance curves (FDCs) in the glassy state reveals separate forms at different locations indicated in Figure 6 (Figure 11): Location 1 represents FDCs from the "tops" of the layer, location 2 corresponds to the very top of the PMA clusters that prod through to within 10 nm of the top of the brush, and location 3 represents an area in which very thin PSF is layered over the top of the PMA cluster. The FDCs, load−penetration curves, and modulus−depth profile plots for location 2 are all characteristic of AFM tip interaction with a compliant surface (Figure 11). The adhesion in the FDCs is larger for location 2, as is the pull-off force necessary to disjoint the tip/sample contact. Because of the polar character of PMA material compared with the fluorinated groups in PSF, the intrinsic difference in surface energies will lead to higher adhesion. The energy required to pull off the surface also increases with the area of mechanical contact, and this will be higher for the compliant PMA. In addition, the slopes of the FDCs are very different for locations 1 and 2, indicating differences in the actual cantilever deflection as it indents into the sample.[48,58] A slope approaching unity describes the situation when the tip feels an infinitely hard surface, such as silicon. Slopes range from 0.6 to 0.8 for location 1 and 0.2 to 0.4 for location 2. Conversion of the FDCs into load−penetration curves further confirms that a more compliant surface is associated with location 2 as indentation is twice as deep under identical normal loads (Figure 11). Depth profiling of the elastic modulus shows a constant value of nearly 1 GPa at location 1. This behavior is in sharp contrast with location 2 as the
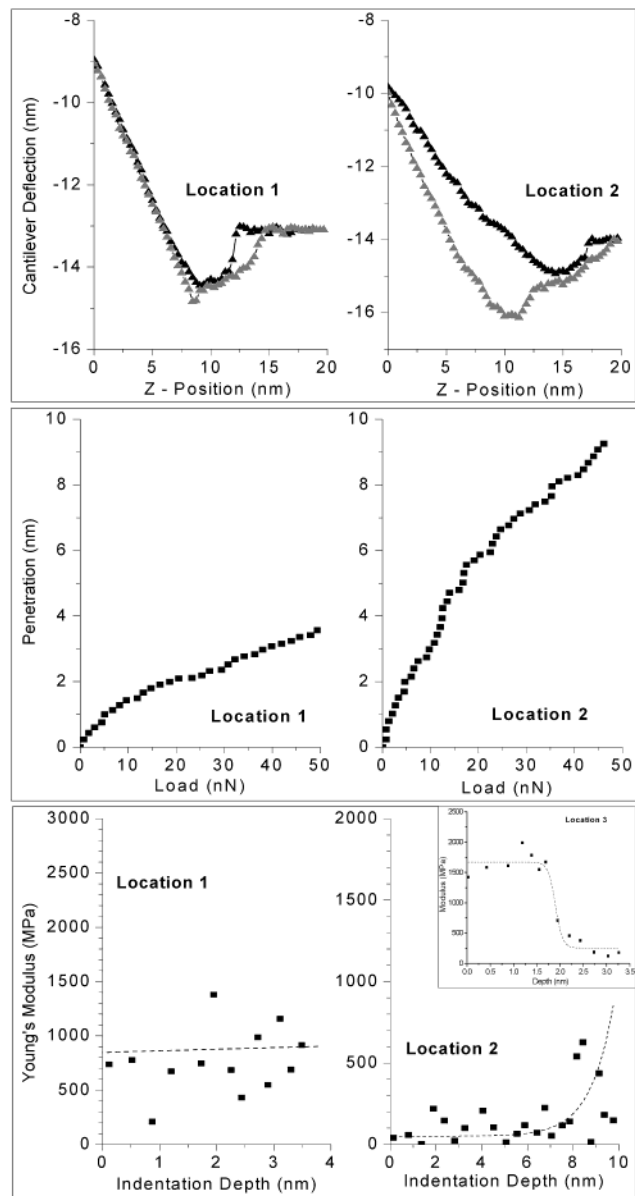
Figure 11. Typical FDCs (top, black triangles indicate approaching cycle, gray triangles indicate retracting cycle), load−penetration (middle), and elastic modulus depth profiles (bottom) for the glassy state. Location 1 and location 2 refer to the points depicted in Figure 6. The inset in bottom right plot shows the depth profile for location 3 from Figure 6 as well.

initial modulus is close to 50 MPa until about 10 nm of penetration, at which point it climbs steeply. This latest behavior is observed for compliant polymer layers on a top of stiff substrate such as silicon oxide or glassy polymer surfaces.[59] It allows determining the elastic modulus of compliant PMA layer (50 MPa) and its thickness (10 nm). These results are consistent with MMA data for PMA homobrush layer and AFM scratch test and indicate PMA material grafted to the silicon substrate. Depth profiling within the depletion (location 3) reveals more complicated shape: a higher elastic modulus was observed for the initial 20 nm and much lower elasticity for larger indentations (Figure 11). Such a shape confirms the two-layered structure of selected areas of binary brushes with a rubbery layer beneath the topmost glassy layer.

   MMA results for the rubbery state are given in Figure 12. FDCs from the "tops" correspond to probing on the
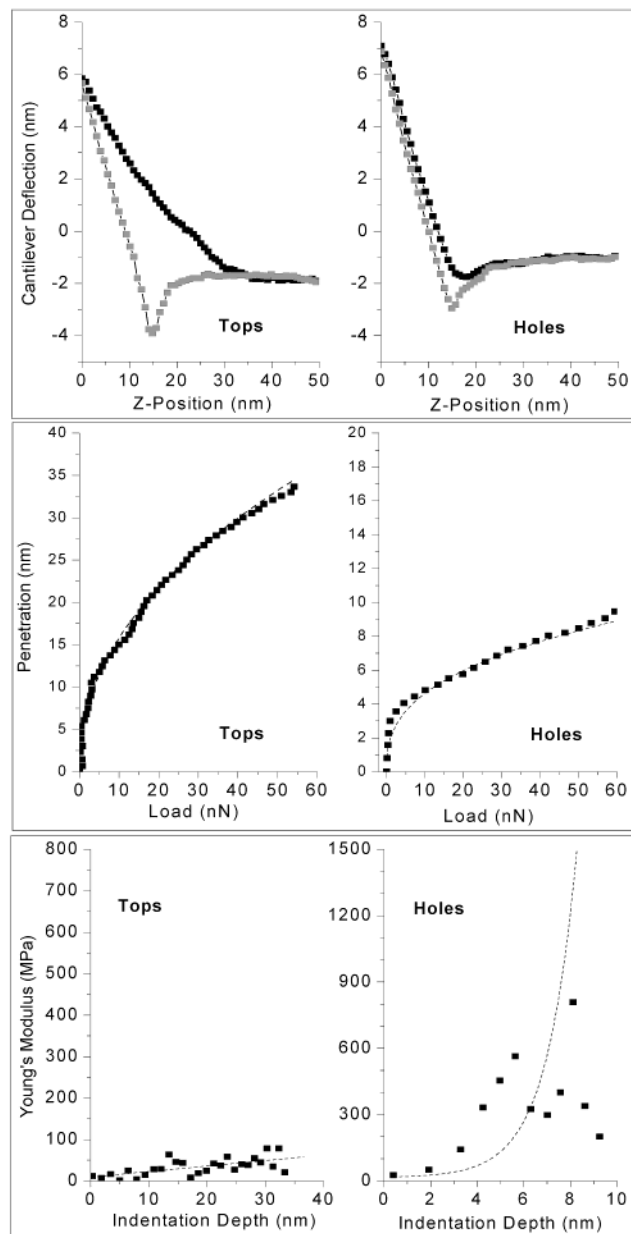

Figure 12. Typical FDCs (top, black squares indicate approaching cycle; gray squares indicate retracting cycle), load−penetration (middle), and elastic modulus depth profiles (bottom) for the rubbery state. "Tops" and "holes" correspond to MMA probing on the PMA weblike structure and PSF dominated surfaces in the 100 nm deep holes, respectively.

weblike structures while "holes" refers to the deep gaps in this structure. For the rubbery state, nearly all FDCs exhibited behavior indicative of a highly compliant surface. Penetration into the PMA was routinely above 30 nm for a load of 50 nN, while for PSF in the glassy state, the deepest penetration was 4 nm for the similar load. Depth profiling of the elastic modulus for the rubbery state showed a steady increase as surface layer was compressed but still did not exceed 70 MPa after 40 nm of indentation (Figure 12). The effect of PSF was felt in the deepest holes as the elastic modulus quickly jumped to roughly 1 GPa after 6 nm of indentation, indicating a thin PMA layer within holes. Therefore, these results confirm the presence of rubbery PMA layer all over the binary brush after acetone exposure.

   Model of Molecular Reorganization. The morphology of the brush layer in the different states based

Table 3. Summary of Reorganization of PSF and PMA Components When the Binary Brush Is Switched

	after toluene exposure (glassy state)		after acetone exposure (rubbery state)	
brush layer	chain organization	AFM scratch test thickness (nm)[a]	chain organization	AFM scratch test thickness (nm)[a]
PMA	collapsed; forms clusters	30–40	swollen; segregates to top of brush	110–120
PSF	swollen; segregates to top of brush	50	collapsed; forms clusters	10–15
PMA + PSF	incomplete layering with dimple structure	50 (2 nm roughness)	complete layering with dimple structure	110–120 (30 nm roughness)

[a] Measured from the cross sections of the brush layers for different surface areas as demonstrated in Figure 7.
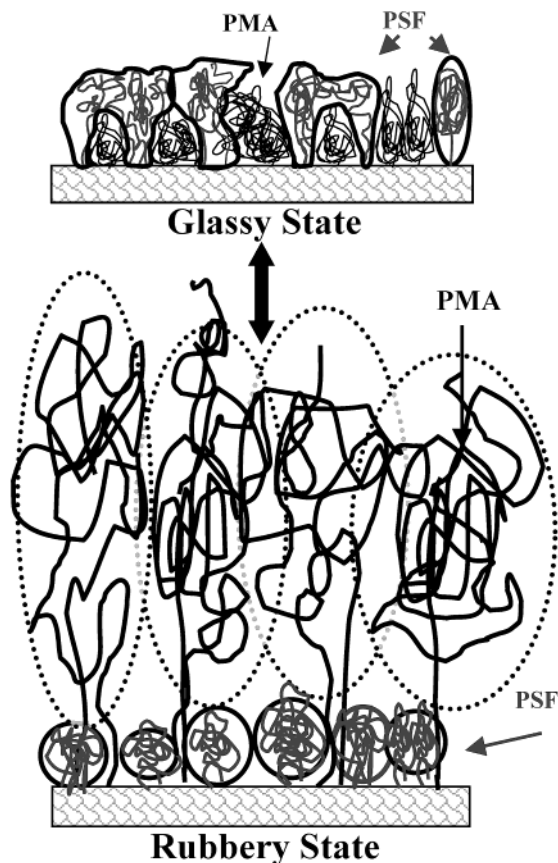

Figure 13. Model depicting the reordering of PSF and PMA chains switching upon exposure to selective solvents (toluene and acetone, respectively). Spheres in the rubbery state are shown to emphasize that there is no free volume, and PMA chains occupy all space above the collapsed PSF layer.

on both AFM imaging and micromechanical testing can be summarized by the model presented in Figure 13. Complete results in terms of the conformation and thickness of each component in both the glassy and rubbery state are summarized in Tables 2 and 3. After exposure to acetone, the brush surface is characterized by dramatic swelling of the PMA phase, and the layered profile dominates with the PSF phase collapsing into clusters to form the dimple structure below PMA layer. Several AFM experiments and theoretical estimations have shown that clusters will form in the collapsed component in the range of medium to high grafting densities. Considering that PSF in this brush should be in the medium to high grafting density range, the suggested formation of the dimple PSF phase in the rubbery state seems to be justified.[60–63]

After exposure to toluene, PSF swells and the layered phase is observed with PSF forming a nearly complete layer over the collapsed PMA (Figure 13). Only in the deepest holes can the top of the PMA dimples be detected. The intermediate holes of 1–8 nm deep are merely depressions in the PSF topmost layer. According to recent theoretical calculations, the collapsed PMA dimples should form into a hexagonal lattice[25] but Fourier transform of the image indicated only usual short-range ordering. From AFM scratch tests, PMA went from a height of 100–120 nm down to cluster sizes of 30 nm height after exposure to bad solvent (Figure 13). Our results indicate that in both the glassy and rubbery states a combination of the layer and dimple phases occurs. The selective solvent greatly enhances the vertical (layering) segregation of a particular phase, while the other component collapses into the dimple structure beneath. This is in agreement with recent theoretical predictions and experiments for a binary polymer brush composed of two highly incompatible polymers.[25,43] MMA results clearly confirm the complete change of the mechanical response in the binary brush after exposure to different selective solvents.

References and Notes

(1) Muller, R. S. In *Micro/Nanotribology and Its Applications*; Bhushan, B., Ed.; Kluwer Academic Press: Dordecht, 1997; p 579. *Tribology Issues and Opportunities in MEMS*; Bushan, B., Ed.; Kluwer Academic Publishers: Dordrecht, 1997. Tsukruk, V. V. In *Nanotribology*; Hsu, S. M., Ying, C. Z., Eds.; Kluwer Academic Press: Boston, 2002; p 347.

(2) Halperin, A.; Tirrell, M.; Lodge, T. P. *Adv. Polym. Sci.* **1992**, *100*, 33. Milner, S. T. *Science* **1991**, *251*, 905. Klein, J. *Annu. Rev. Mater. Sci.* **1996**, *26*, 581.

(3) Granick, S. In *Physics of Polymer Surfaces and Interfaces*; Sanchez, I., Ed.; Manning: New York, 1993.

(4) Sperling, L. H. *Introduction to Physical Polymer Science*, 3rd ed.; Wiley-Interscience: New York, 2001.

(5) Alexander, S. J. *J. Phys. (Paris)* **1977**, *38*, 977.

(6) de Gennes, P. G. *Macromolecules* **1980**, *13*, 1069.

(7) Karim, A.; Tsukruk, V. V.; Douglas, J. F.; Satija, S. K.; Fetters, L. J.; Reneker, D. H.; Foster, M. D. *J. Phys., II* **1995**, *5*, 1441. Tsukruk, V. V. *Prog. Polym. Sci.* **1997**, *22*, 247.

(8) Zhao, B.; Brittain, W. J. *Prog. Polym. Sci.* **2000**, *25*, 677. Zhao, B.; Brittain, W. J. *J. Am. Chem. Soc.* **1999**, *121*, 3557. Zhao, B.; Brittain, W. J.; Zhou, W.; Cheng, S. Z. D. *J. Am. Chem. Soc.* **2000**, *122*, 2407. Sedjo, R.; Mirous, B.; Brittain, W. J. *Macromolecules* **2000**, *33*, 1492.

(9) Wittmer, J.; Johner, A.; Joanny, J. F. *Colloids Surf. A: Physiochem. Eng. Aspects* **1994**, *86*, 85.

(10) Israëls, R.; Leermakers, F. A. M.; Fleer, G. J.; Zhulina, E. B. *Macromolecules* **1994**, *27*, 3249.

(11) Takei, Y. G.; Aoki, T.; Sanui, K.; Ogata, N.; Sakurai, Y.; Okanao, T. *Macromolecules* **1994**, *27*, 6163.

(12) Auroy, P.; Auvray, L.; Leger, L. *Phys. Rev. Lett.* **1991**, *66*, 719.

(13) Raviv, U.; Tadmor, R.; Klein, J. *J. Phys. Chem. B* **2001**, *105*, 8125.

(14) Grest, G. S.; Murat, M. *Macromolecules* **1993**, *26*, 3108.

(15) Pincus, P. *Macromolecules* **1991**, *24*, 2912.

(16) Galaev, I.; Mattiasson, B. *Trends Biotechnol.* **1999**, *17*, 335.
(17) Aksay, A.; Trau, M.; Manne, S.; Honma, I.; Yao, N.; Zhou, L.; Fenter, F.; Eisenberger, P. M.; Gruner, S. M. *Science* **1996**, 273.
(18) Ito, Y.; Ochiai, Y.; Park, Y. S.; Imanishi, Y. *J. Am. Chem. Soc.* **1997**, *119*, 1619.
(19) Leger, L.; Raphaël, E.; Hervert, H. *Adv. Polym. Sci.* **1999**, *138*, 185.
(20) Ruths, M.; Johannsmann, D.; Rühe, J.; Knoll, W. *Macromolecules* **2000**, *33*, 3860.
(21) Mansky, P.; Liu, Y.; Huang, E.; Russell, T. P.; Hawker, C. J. *Science* **1997**, *275*, 1458.
(22) Marko, J. F.; Witten, T. A. *Phys. Rev. Lett.* **1991**, *66*, 1541.
(23) Soga, K. G.; Zuckermann, M. J.; Guo, H. *Macromolecules* **1996**, *29*, 1998.
(24) Brown, G.; Chakrabarti, A.; Marko, J. F. *Europhys. Lett.* **1994**, *25*, 239.
(25) Müller, M. *Phys. Rev. E* **2002**, *65*, 30802.
(26) Minko, S.; Patil, S.; Datsyuk, V.; Simon, F.; Eichorn, K. J.; Motornov, M.; Usov, D.; Tokarev, I.; Stamm, M. *Langmuir* **2002**, *18*, 289.
(27) Luzinov, I.; Julthongpiput, D.; Malz, H.; Pionteck, J.; Tsukruk, V. V. *Macromolecules* **2000**, *33*, 1043.
(28) Luzinov, I.; Julthongpiput, D.; Tsukruk, V. V. *Macromolecules* **2000**, *33*, 7629.
(29) Biebuyck, H. A.; Bain, C. D.; Whitesides, G. M. *Langmuir* **1994**, *10*, 1825. Folkers, J. P.; Gorman, C. B.; Laibinis, P. E.; Buchholz, S.; Whitesides, G. M. *Langmuir* **1995**, *11*, 813. Lee, T. R.; Carey, R. I.; Biebuyck, H. A.; Whitesides, G. M. *Langmuir* **1994**, *10*, 741.
(30) Ulman, A. *Chem. Rev.* **1996**, *96*, 1533.
(31) Xue, G.; Joenig, J. L.; Ishida, H.; Wheeler, D. D. *Rubber Chem. Technol.* **1991**, *64*, 162. Noy, I. A.; Vezenov, D. V.; Lieber, C. M. *Annu. Rev. Mater. Sci.* **1997**, *27*, 381. Tsukruk, V. V.; Bliznyuk, V. N. *Langmuir* **1998**, *14*, 446. Tsukruk, V. V.; Lander, L. M.; Brittain, W. J. *Langmuir* **1994**, *10*, 996.
(32) Tsukruk, V. V.; Luzinov, I.; Julthongpiput, D. *Langmuir* **1999**, *15*, 3029. Luzinov, I.; Julthongpiput, D.; Liebmann-Vinson, A.; Cregger, T.; Foster, M. D.; Tsukruk, V. V. *Langmuir* **2000**, *16*, 504.
(33) Prucker, O.; Naumann, C. A.; Rühe, J.; Knoll, W.; Franck, C. W. *J. Am. Chem. Soc.* **1999**, *121*, 8766.
(34) Sidorenko, A.; Minko, S.; Schenk-Meuser, K.; Duschner, H.; Stamm, M. *Langmuir* **1999**, *15*, 8349.
(35) Luzinov, I.; Voronov, A.; Minko, S.; Kraus, R.; Wilke, W.; Zhuk, A. *J. Appl. Polym. Sci.* **1996**, *61*, 7/1101.
(36) Minko, S.; Gafijchuk, G.; Sidorenko, A.; Voronov, S. *Macromolecules* **1999**, *32*, 4525.
(37) Minko, S.; Sidorenko, A.; Stamm, M.; Gafijchuk, G.; Senkovsky, V.; Voronov, S. *Macromolecules* **1999**, *32*, 4532.
(38) Boven, G.; Oosterling, M. L. C. M.; Chall, G.; Schouten, A. J. *Polymer* **1990**, *31*, 2377.
(39) Prucker, O.; Rühe, J. *Macromolecules* **1998**, *31*, 592.
(40) Prucker, O.; Rühe, J. *Macromolecuels* **1998**, *31*, 602.
(41) Lemieux, M.; Minko, S.; Usov, D.; Stamm, M.; Tsukruk, V. V. *Langmuir* **2003**, *19*, 6126.
(42) Minko, S.; Usov, D.; Goreshnik, E.; Stamm, M. *Macromol. Rapid Commun.* **2001**, *22*, 206.
(43) Minko, S.; Müller, M.; Usov, D.; Scholl, A.; Froeck, C.; Stamm, M. *Phys. Rev. Lett.* **2002**, *88*, 5502.
(44) Tsukruk, V. V. *Rubber Chem. Technol.* **1997**, *70*, 430. Tsukruk, V. V.; Reneker, D. H. *Polymer* **1995**, *36*, 1791.
(45) Cappella, B.; Dietler, G. *Surf. Sci. Rep.* **1999**, *34*, 1.
(46) *Scanning Probe Microscopy of Polymers*; Ratner, B., Tsukruk, V. V., Eds.; ACS Symposium Series; American Chemical Society: Washington, DC, 1998; Vol. 694.
(47) *Microstructure and Microtribology of Polymer Surfaces*; Tsukruk, V. V., Wahl, K., Eds.; American Chemical Society: Washington, DC, 1999; Vol. 741.
(48) Tsukruk, V. V.; Gorbunov, V. V. *Probe Microsc.* **2002**, *3−4*, 241. Huang, Z.; Chizhik, S. A.; Gorbunov, V. V. *J. Mater. Sci.* **1998**, *33*, 4905. Tsukruk, V. V.; Huang, Z. *Polymer* **2000**, *41*, 5541.
(49) Hazel, J. L.; Tsukruk, V. V. *Thin Solid Films* **1999**, *339*, 249.
(50) Hazel, J. L.; Tsukruk, V. V. *J. Tribol.* **1998**, *120*, 814.
(51) Radmacher, M.; Tillmann, R. W.; Gaub, H. E. *Biophys. J.* **1993**, *64*, 735.
(52) Tsukruk, V. V.; Gorbunov, V. *Microsc. Today* **2001**, *01-1*, 8.
(53) *Polymer Handbook*, 4th ed.; Brandrup, J., Immegurt, E. H., Grulke, E. A., Eds.; John Wiley & Sons: New York, 1999.
(54) Extrand, C. W. *Langmuir* **2002**, *18*, 7991.
(55) Magonov, S. N.; Cleveland, J.; Elings, V.; Denley, B.; Whangbo, M. H. *Surf. Sci.* **1997**, *389*, 201.
(56) Berquand, A.; Mazeran, P. E.; Laval, J. M. *Surf. Sci.* **2003**, *523*, 125.
(57) Tsukruk, V. V.; Gorbunov, V.; Luzinov, I.; Huang, Z.; Fuchigami, N. In *Interfacial Properties on the Submicrometer Scale*; Frommer, J., Overney, R. M., Eds.; ACS Symposium Series; American Chemical Society: Washington, DC, 2001; Vol. 781, p 254. Tsukruk, V. V.; Gorbunov, V. V.; Huang, Z.; Chizhik, S. A. *Polym. Int.* **2000**, *49*, 441.
(58) Luzinov, I.; Julthongpiput, D.; Bloom, P. D.; Sheares, V. V.; Tsukruk, V. V. *Macromol. Symp.* **2001**, *167*, 229. Chizhik, S. A.; Gorbunov, V. V.; Fuchigami, N.; Luzinov, I.; Tsukruk, V. V. *Macromol. Symp.* **2001**, *167*, 169.
(59) Tsukruk, V. V.; Shulha, H.; Zhai, X. *Appl. Phys. Lett.* **2002**, *80*, 4825. Tsukruk, V. V.; Sidorenko, A.; Gorbunov, V. V.; Chizhik, S. A. *Langmuir* **2001**, *17*, 6715. Tsukruk, V. V.; Shulha, H.; Zhai, X. *Appl. Phys. Lett.* **2003**, *82*, 907. Tsukruk, V. V. *Adv. Mater.* **2001**, *13*, 95.
(60) Koutos, V.; van der Vegte, E. W.; Hadziioannou, G. *Langmuir* **1999**, *32*, 1233.
(61) Koutos, V.; van der Vegte, E. W.; Pelletier, E.; Stamouli, A.; Hadziioannou, G. *Langmuir* **1997**, *30*, 4719.
(62) Siqueira, D. F.; Kohler, K.; Stamm, M. *Langmuir* **1995**, *11*, 3092.
(63) Zhulina, E. B.; Birshtein, T. M.; Priamitsyn, V. A.; Klushin, L. I. *Macromolecules* **1995**, *28*, 8612.